applied sciences

MDPI

Article

Numerical Analysis of the Detailed Balance of Multiple Exciton Generation Solar Cells with Nonradiative Recombination

Jongwon Lee * and Christiana B. Honsberg

School of Electrical, Computer and Energy Engineering, Arizona State University, Tempe, AZ 85287, USA; honsberg@asu.edu

* Correspondence: jlee159@asu.edu

Received: 4 July 2020; Accepted: 8 August 2020; Published: 11 August 2020

Abstract: In this study, we analyzed the nonradiative recombination impact of multiple exciton generation solar cells (MEGSCs) with a revised detailed balance (DB) limit. The nonideal quantum yield (QY) of a material depends on the surface defects or the status of the material. Thus, its QY shape deviates from the ideal QY because of carrier losses. We used the ideal reverse saturation current variation in the DB of MEGSCs to explain the impact of nonradiative recombination. We compared ideal and nonideal QYs with the nonradiative recombination into the DB of MEGSCs under one-sun and full-light concentration. Through this research, we seek to develop a strategy to maintain MEGSC performance.

Keywords: multiple exciton generation; impact ionization; detailed balance; quantum yield

1. Introduction

Multiple exciton generation solar cells (MEGSCs) are promising future-generation solar cells that are capable of creating several electron and hole pairs (EHPs) via impact ionizations. This can overcome the theoretical single-junction efficiency limit by decreasing the carrier thermalization loss in nanostructured materials [1–3].

A quantum efficiency of >100% has been observed in silicon solar cells, which has motivated the development of theoretical and empirical approaches for MEGSCs [4,5]. The theoretical efficiency of MEGSCs has been calculated [5–9] based on the ideal quantum yield (QY), which is the number of EHPs generated under blackbody radiation.

In the detailed balance (DB) limit, single-junction solar cells (SJSCs) consider only one radiative recombination (Figure 1a), and the MEGSC undergoes multiple-carrier recombination (MR) via Auger recombination (AR). The $M - 1$ electrons directly recombine into holes and transfer their energy to the remaining electron, where M is the maximum generated EHPs. By absorbing the energy, the electron excites to a high-energy state. Thereafter, it emits single-photon energy (which is equal to the product of the maximum quantum yield and the bandgap energy) without losses (Figure 1b) [7]. The amount of photon energy emitted is comparable to that of the topmost junction in a tandem solar cell under blackbody radiation. An MEGSC under blackbody radiation shows efficient carrier management, undergoing no other nonradiative recombination processes. However, the MR in the actual materials describes nonradiative AR to occur via phonon-assisted electron or hole relaxation [10] (Figure 1c). Experiments show that the excited electrons or holes release their kinetic energy to reach the valence band. Subsequently, the carrier experiences direct recombination or capture at the trap. Therefore, this relaxation process limits the performance of an MEGSC as the carrier cooling rate is slowed down, moving from one state to another [11]. In the context of carrier dynamics of the MEGSC theory, the excited carriers experience multiple exciton generation (MEG) via impact ionization, release energy via phonons, and produce additional decay paths through surface state or defects. Thus, these conditions produce a less-ideal MEG because of the generation of nonradiative recombination paths of quantum dots (QDs) in MEGSCs [11].

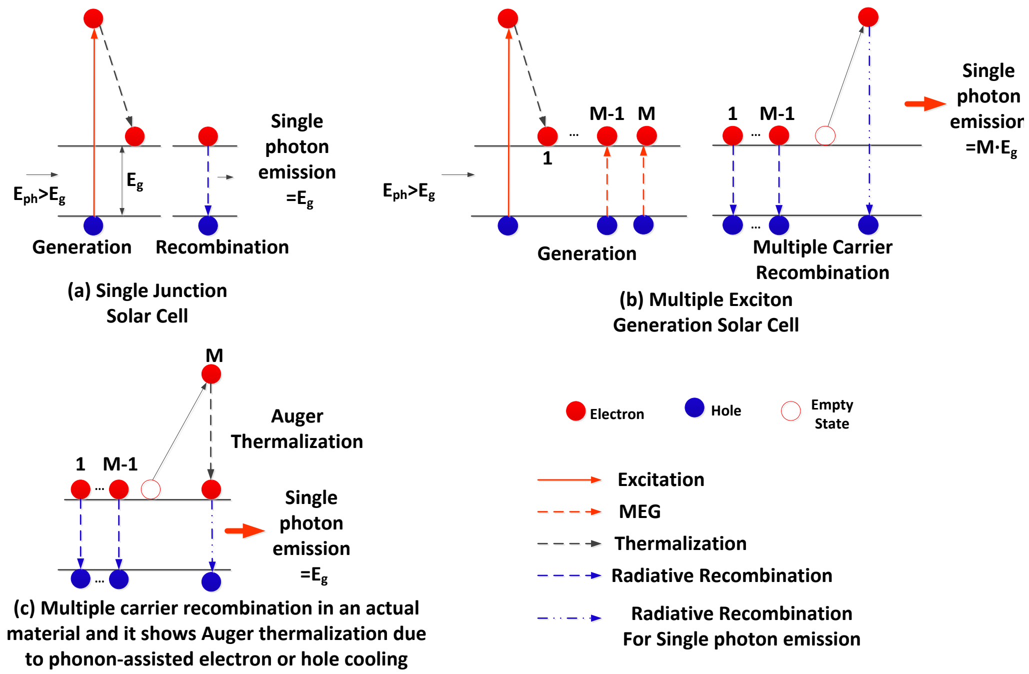

Figure 1. Carrier generation and recombination process of a single-junction solar cell (SJSC) and multiple exciton generation solar cell (MEGSC). (**a**) One electron and hole pair (EHP) generation and recombination of SJSC. (**b**) Multiple EHP generation process by impact ionization and multiple carrier recombination process after Auger recombination (AR) where M is the maximum generated EHPs (1, 2, 3, . . . , M − 1, M). (**c**) Multiple carrier recombination and Auger thermalization via phonon-assisted electron or hole cooling after a carrier excitation.

The discrepancy between ideal and actual performance depends on MEGSC idealities. Two parameters are crucial to test the characteristics of an MEGSC: QY and threshold energy (= E_{th}). The ideal quantum yield (IQY) increases according to a staircase step function, and the threshold energy describes the onset point over 100% of QY. The E_{th} for IQY is twice that of the bandgap energy ($E_{th} = 2 \cdot E_g$) without carrier losses [5–9], but the actual material shows a difference in QY and E_{th} because of nonidealities related to surface state or defects. Thus, the nonideal quantum yield (NQY) shows a delayed E_{th} and a linearly increasing QY. During initial measurements of QY in PbSe QDs up to 300% and 700% [12,13], various groups have examined the NQY by pump–probe measurements with CdTe [14], CdSe [15], InAs [16,17], and Si [18]. The uncertainties related to surface states and long-lived QD photocharging in the pump–probe measurements [19,25] have limited the QY up to 300% in QD systems. The experimental results of measurements in QD MEGSCs are much lower than the theoretical limit owing to nonradiative recombination and insufficient light absorption [26–30]. Therefore, these shortcomings have initiated developments in the DB limit of an MEGSC for quantitative analysis of the impact of nonradiative recombination.

The conventional AR depends on the material parameters (carrier lifetime, doping concentration, and Auger constant) in the DB [31]. To generalize the nonradiative recombination, the rate-based calculation of DB considers the nonradiative generation and recombination and its ideal reverse saturation current [1]. Thus, the SJSC can be made to achieve a semiempirical limit by varying the ideal reverse saturation current, which helps explain the nonradiative recombination impacts [1]. Therefore, this method can be applied to the DB of MEGSC.

In this paper, we present a study on the DB limit of an MEGSC, which involves a quantitative analysis of the nonradiative recombination impact. For simulation purposes, we altered the DB of MEGSC by varying the ideal reverse saturation current (J_0) from the nonradiative generation and recombination in order to derive the ideal reverse saturation condition for MEGSC. By varying this parameter, we were able to obtain a semiempirical limit and discuss the impact of the nonradiative recombination of MEGSC.

2. Theory

2.1. Detailed Balance Equations of the MEG

The DB equations of the MEG are represented by Equations (1) to (5). QY is the most crucial parameter for determining all the characteristics of the MEG [5–9]. Both the IQY (QY = 14; Figure 1a) and NQY ($E_{th,}$ from $2E_g$ to $4E_g$; Figure 1b) are shown in Equation (1) and Figure 2. The IQY follows a step function with a full generation of multiple EHPs per photon. The actual QY (the NQY case) extracted from the pump–probe measurements shows a deviation from the IQY after reaching the E_{th} [12–25,32]. In the pump–probe measurements, the NQY is induced from the scale of the transient absorption signals (peak intensities and their decay signals). While pump intensities between multiple EHPs (high peak) and a single EHP (bleach signal) are compared, certain phenomena can be analyzed at the point of reaching E_{th} in MEG, the potential number of generated EHPs, and MEG efficiency (the increment of additional EHPs by applied intensities) [11,12,33]. The modeling and related equations are reported in [12,30,34–36].

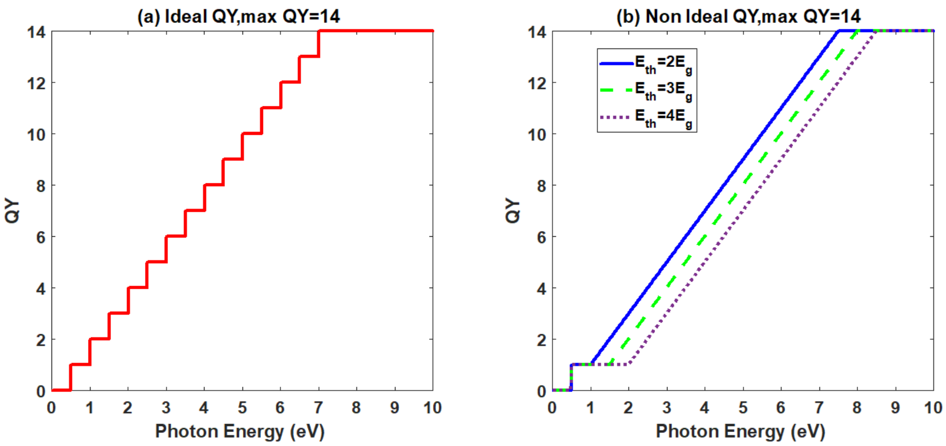

Figure 2. Ideal quantum yield (IQY) (maximum QY = 14) and nonideal quantum yields (NQYs) with three different threshold energies (2Eg, 3Eg, and 4Eg), where Eg = 0.5 eV.

In NQY, E_{th} is a significant parameter that explains the carrier extraction of MEGSCs (E_{th}: the onset point of QY over 100%). The delayed E_{th} ($>2E_g$) requires a higher photon energy for MEG and describes the status of MEG materials. Typically, E_{th} depends on the effective mass of electrons and holes in a material. The surface state has a large impact on the MEG process because of fast carrier decay, which creates other decay paths at trap states [12]. Therefore, creating a near-perfect MEGSC is the first priority for maintaining its idealities.

To ensure minimal or no mathematical errors, the open-circuit voltage (V_{OC}) must be less than the bandgap energy. QY in Equation (5) relates to the generated number of EHPs for MEG, the excited high-energy state, and its photon energy emission through radiative recombination without losses. For instance, the optimum bandgap is 0.05 eV with QY = 200 and C = 46,200 suns. When 199 electrons recombine into holes, the energy is transferred to the 200th electron. This excites the electron to an energy state of 10 eV and causes the emission of photon energy without losses under blackbody radiation [6]. However, conventional AR is the nonradiative recombination in actual materials and uses an alternative DB in silicon solar cells [10,31]. Thus, the MEGSC theory only considers blackbody radiation [6–8].

$$
\begin{aligned}
&\text{Ideal} \quad QY(E) = \begin{cases} 0 & 0 < E < E_g \\ m & m \cdot E_g < E < (m+1) \cdot E_g \quad m = 1, 2, 3, \cdots \\ M & E \geq M \cdot E_g \end{cases} \\
&\text{Non} \quad \text{Ideal} \quad QY(E) == \begin{cases} 0 & 0 < E < E_g \\ 1 & E_g < E < E_{th} \cdot E_g \\ 1 + \cdot A \cdot (\frac{E - E_{th}}{E_g}) & E \geq E_{th} \cdot E_g \end{cases}
\end{aligned} \tag{1}
$$

where m is the number of multiple EHPs generated, M is the maximum number of EHPs, E_g is the bandgap, and E is the photon energy. A (=1) is the slope of the linearized QY, and E_{th} is the threshold energy for an MEG event.

$$
\phi(E_1, E_2, T, \mu) = \frac{2\pi}{h^3 c^2} \int_{E_1}^{E_2} \frac{E^2}{\exp[(E - \mu)/kT] - 1} dE \tag{2}
$$

$$
\phi_{MEG}(E_1, E_2, T, \mu) = \frac{2\pi}{h^3 c^2} \int_{E_1}^{E_2} \frac{QY(E) \cdot E^2}{\exp[(E - \mu_{MEG})/kT] - 1} dE \tag{3}
$$

$$
\begin{aligned}
J_{BB} \quad &= q \cdot C \cdot f_s \cdot \phi_{MEG}\big(E_g, \infty, T_S, 0\big) \\
&+ q \cdot C \cdot (1 - f_s) \cdot \phi_{MEG}\big(E_g, \infty, T_C, 0\big) \\
&- q \cdot \phi_{MEG}\big(E_g, \infty, T_C, \mu_{MEG}\big)
\end{aligned} \tag{4}
$$

$$
\mu_{MEG} = q \cdot QY(E) \cdot V \tag{5}
$$

where ϕ is the particle flux given by Planck's equation for a temperature T, with a chemical potential (CP) μ in the photon energy range E_1–E_2; h is Planck's constant; c is the speed of light in vacuum; and μ is the CP of an SJSC (q·V), where V is the operating voltage. μ_{MEG} is the CP of MEG (q·QY(E)·V), k is the Boltzmann constant, J is the current density of the solar cell, q is the element of the charge, C is the optical concentration, f_S is the geometry factor (1/46,200), T_S is the temperature of the sun (6000 K), and T_C is the temperature of the solar cell (300 K).

2.2. Numerical Analysis of the Nonradiative Recombination of an MEGSC

The deviation in QY depends on the material properties, such as effective mass, surface states, or defects of QD materials [37]. Thus, NQY describes the loss of EHPs from m·E_g to (m + 1)·E_g. To account for this, we reconfigured the DB of the MEGSC to include nonradiative recombination [1].

In the rate-based calculations, the DB of MEG is shown in Equation (6) [1]:

$$
F_{s,MEG} - F_{c,MEG}(V) + R_{MEG}(0) - R_{MEG}(V) - J_{BB}/q = 0 \tag{6}
$$

where $F_{S,MEG}$ and $F_{C,MEG}(V)$ are the generation and recombination for the radiative term, respectively, and $R_{MEG}(0)$ and $R_{MEG}(V)$ are the nonradiative generation and recombination, respectively [1].

Equation (6) is reordered to show the net rate of generation and recombination in Equation (7) [1].

$$
\begin{aligned}
&F_{s,MEG} - F_{c0,MEG} + \\
&[F_{c0,MEG} - F_{c,MEG}(V) + R_{MEG}(0) - R_{MEG}(V)] - J_{BB}/q = 0
\end{aligned} \tag{7}
$$

To show the radiative and nonradiative limits, the following change is made to the part of Equation (7) inside brackets [1]:

$$\begin{aligned} &F_{c0,MEG} - F_{c,MEG}(V) \\ &= f_{NR} \cdot [F_{c0,MEG} - F_{c,MEG}(V) + R_{MEG}(0) - R_{MEG}(V)] \end{aligned} \tag{8}$$

where f_{NR} denotes the ratio between radiative recombination and nonradiative recombination, which indicates the contribution of radiative recombination in the MEGSC [1].

If the nonradiative recombination fits the ideal rectifying equation, f_{NR} can show the ideal reverse saturation current (J_0) (Equation (9)) [1]:

$$f_{NR} = \frac{F_{c0,MEG}}{F_{c0,MEG} + R_{MEG}(0)} = \frac{F_{c0,MEG}}{J_0} \tag{9}$$

where $0 < f_{NR} \le 1$ and $J_0 = (F_{C0,MEG} + R_{MEG}(0))$.

In an ideal rectifying diode, J_0 is a voltage-dependent parameter. Therefore, the term for the recombination current, $\exp(q{\cdot}QY{\cdot}V/k{\cdot}T_C)$, is included as shown in Equation (10):

$$\begin{aligned} J_{BB} = {} & q \cdot (F_{s,MEG} - F_{c0,MEG}) \\ & + q \cdot (F_{c0,MEG}/f_{NR})\left[1 - \exp\left(\tfrac{q \cdot QY \cdot V}{k \cdot T_C}\right)\right] \\ & = q \cdot (F_{s,MEG} - F_{c0,MEG}) + J_0 \cdot \left[1 - \exp\left(\tfrac{q \cdot QY \cdot V}{k \cdot T_C}\right)\right] \end{aligned} \tag{10}$$

where $F_{S,MEG} = C{\cdot}f_S{\cdot}\phi_{MEG}(E_g,\infty,T_S,0) + C{\cdot}(1 - f_S){\cdot}\phi_{MEG}(E_g,\infty,T_C,0)$, and $F_{C0,MEG} = \phi_{MEG}(E_g,\infty,T_C,0)$.

In the DB equations above, V_{OC} depends on f_{NR}, which decreases as J_0 increases. Its equation is shown in Equation (11). This leads to reduced theoretical efficiencies by increased nonradiative recombination for producing a smaller fraction of radiative recombination [1].

$$V_{OC} = \frac{k \cdot T_c}{q} \cdot \ln\left[f_{NR} \cdot \frac{F_{S,MEG}}{F_{C0,MEG}} - f_{NR} + 1\right] \tag{11}$$

The correlated theoretical efficiency is shown in Equation (12):

$$\eta(\text{Efficiency}) = \frac{J_{BB}(mpp) \cdot V(mpp)}{P_{in}\ \ (= C \cdot f_s \cdot \sigma \cdot T_S^4)} \tag{12}$$

where mpp is the maximum power point, P_{in} is the input power, and σ is the Stefan–Boltzmann constant ($= 2\pi^5k^4/(15c^2h^3) = 5.670373 \times 10^{-8}\ Wm^{-2}K^{-4}$).

A similar approach has been discussed for nonradiative recombination in QD solar cells. This involves investigating the external radiative efficiency (ERE) and V_{OC} [38]. The ERE parameter depends on the radiative and nonradiative recombination rates, which affect the voltage losses of quantum dot solar cells (QDSCs). Smaller ratios of ERE reduce the maximum available operating voltage. The voltage losses on QD GaAs or perovskite solar cells have also been discussed [38–40]. Further, the current results of QDSCs have achieved 16.6% efficiency of $Cs_{1-x}FA_xPbI_3$ QDSCs by minimal nonradiative recombination [41].

3. Results and Discussion

We tested seven cases of f_{NR} (10^{-10}, 10^{-5}, 10^{-4}, 10^{-3}, 10^{-2}, 10^{-1}, and 1) to see the impact of nonradiative recombination. The results are summarized in Figures 3–5, Tables S1 and S2, and Figures S1 and S2 (in the supplementary materials). J_0 is inversely proportional to f_{NR} (Equation (9)). A small f_{NR} represents a high nonradiative recombination rate. For all cases, $f_{NR} = 1$ is the case for the IQY of MEGSC. We used both IQY (see Figures 3–5, Table S1, and Figures S1a and S2a) and NQY under one-sun (C = 1; Figures 3a and 4, Table S1, and Figure S1b–d) and full-light concentration (C = 46,200;

Figures 3b and 5, Table S2, and Figure S2b–d). For NQY, we chose E_{th} = $2E_g$, $3E_g$, and $4E_g$ to determine the impact of the nonradiative recombination. Equation (10) can predict the status of the QD MEGSC with NQY because of the nonidealities in the DB of an MEGSC. The MEGSC effect disappears after f_{NR} = 10^{-3} (1000 times J_0) (Figure 3a). We determined the critical point to maintain MEGSC at f_{NR} = 10^{-2} and E_{th} = $2E_g$ under one-sun illumination (Figure 3a and Figure S1b). Finally, increasing the light concentration shifts the critical point (from MEG to SJSC) after f_{NR} = 10^{-5} (10^5 of J_0) for both IQY and NQY (Figures 3b and 5d and Figure S2).

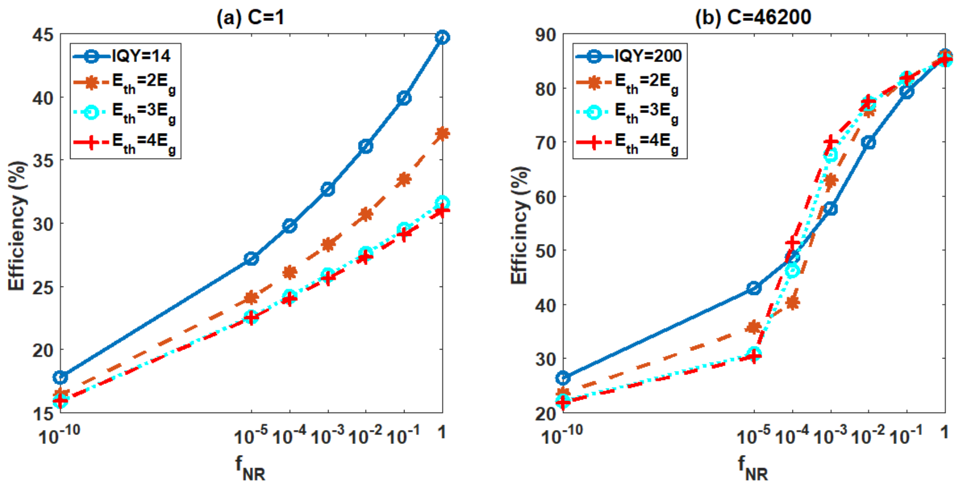

Figure 3. Theoretical maximum efficiency vs. variation of f_{NR} (= 10^{-10},10^{-5},10^{-4},10^{-3},10^{-2},10^{-1},1). For this simulation, we used ideal quantum yield (IQY) and with three different threshold energies (E_{th} = $2E_g$, $3E_g$, and $4E_g$) for NQY.

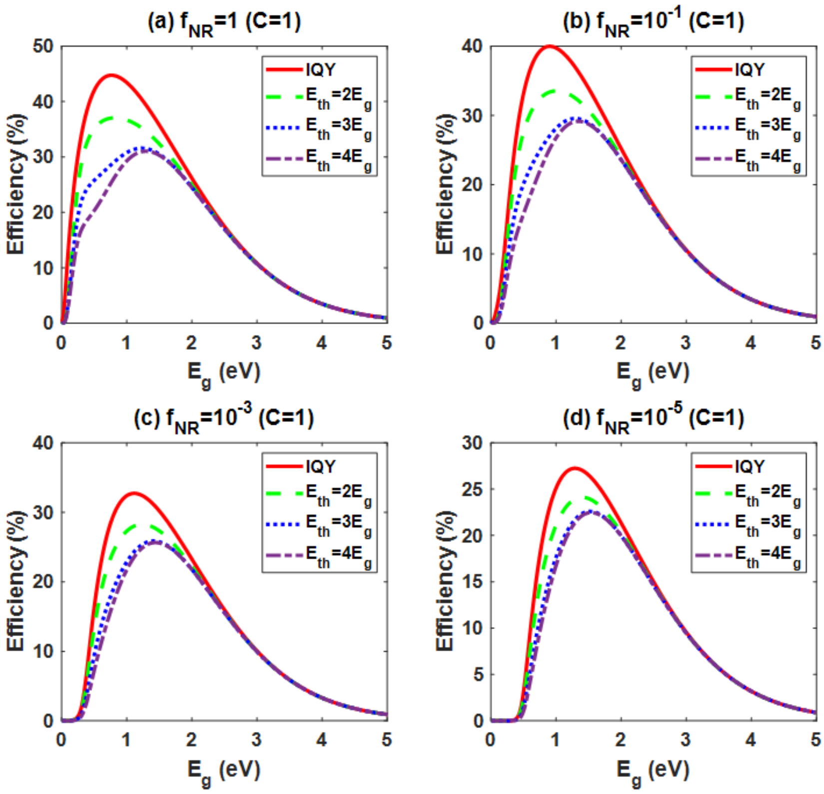

Figure 4. E_g vs. theoretical efficiencies of the MEGSC with fixed f_{NR} under one-sun illumination (C = 1). For this simulation, we used IQY and NQY (E_{th} = $2 \cdot E_g$, $3 \cdot E_g$, $4 \cdot E_g$). f_{NR} is 1, 10^{-1}, 10^{-3}, and 10^{-5}).

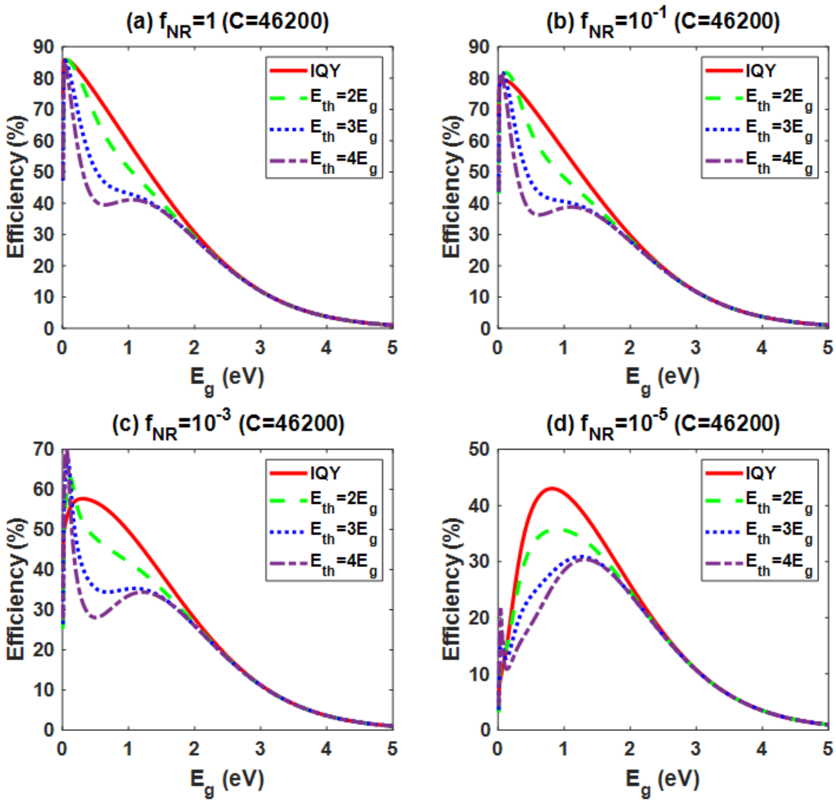

Figure 5. E_g vs. theoretical efficiencies of the MEGSC with fixed f_{NR} under full-light concentration (C = 46,200) For this simulation, we used IQY and NQY (E_{th} = 2·E_g, 3·E_g, 4·E_g). f_{NR} is 1, 10^{-1}, 10^{-3}, and 10^{-5}).

NQY under light-concentration conditions shows dual peaks after E_{th} = 3·E_g (Figure 5 and Figure S2b–d). This represents the transition from the MEGSC to the SJSC, where the first peak is for the MEGSC and the second peak is for the SJSC. Thus, the delayed E_{th} results in less efficient MEGSCs because of the shifting of the optimum point from the MEGSC to an SJSC under light-concentration conditions. Therefore, E_{th} must be maintained at 2·E_g with a low nonradiative recombination rate (e.g., 10 times J_0), typically under one-sun illumination. The material condition for MEGSC is crucial in that the nonradiative recombination impact must be small to maximize the radiative limit. Overall, the results explain the low efficiency of the QD MEGSCs. For instance, the theoretical efficiency is 30.6% for E_g = 0.98 eV at E_{th} = 3E_g when f_{NR} is 1. In the proposed MEGSC detailed balance approach, the theoretical efficiency is 4.6% at $f_{NR} = 10^{-10}$, which is similar to 4.5% for PbSe QDs [27]. We compared other materials such as PbSe and CdTe and summarized the results in Table 1 [27–29]. This shows that even if a QDSC can present excellent conditions for creating multiple EHPs, its high nonradiative recombination decreases the expected results [27–29].

Table 1. Comparison between theoretical efficiency and experimental efficiency of an MEGSC.

This work (Theoretical Efficiency)				Experiment			
E_{th} = 3E_g	f_{NR}	E_g (eV)	η (%)	PbSe [27]	E_{th} = 3E_g	E_g (eV)	η (%)
	10^{-10}	0.98	4.6			0.98	4.5
E_{th} = 3E_g	f_{NR}	E_g (eV)	η (%)	PbSe [28]	E_{th} = 3E_g	E_g (eV)	η (%)
	10^{-11}	0.95	2.1			0.95	1.61
E_{th} = 2.9E_g	f_{NR}	E_g (eV)	η (%)	CdTe [29]	E_{th} = 2.9E_g	E_g (eV)	η (%)
	10^{-11}	0.95	1.38			0.95	1.9

Table 1 presents a comparison of the experimental results (PbSe [27,28] and CdTe [29]) and MEGSC DB approaches considering the effect of nonradiative recombination. For this simulation, we used the ratio of f_{NR} up to 10^{-12} to find an appropriate range of f_{NR} to compare with the low experimental results of an MEGSC. These results indicate low efficiencies of the colloidal QDs of an MEGSC due to the high nonradiative recombination.

As shown in Figure 3 and Table S1, and in agreement with a previous study that used ERE approaches in GaAs QD solar cells [38], we detected similarities between the MEGSC DB and the experimental results. If the GaAs QD bandgap is 1.4–1.5 eV, the efficiency range at $f_{NR} = 10^{-4}$ and 10^{-5} is 23%–25%. These values show similar efficiency ranges at 10^{-4}–10^{-5} of ERE, even if the GaAs QD solar cell does not consider the MEG effects [38]. A small ratio of ERE has a significant impact on V_{oc} owing to the increased nonradiative recombination rate. For instance, if the ERE is in the order of 10^{-8}, the overall voltage drop in V_{OC} is 0.5–0.6 V. Thus, its corresponding efficiency also decreases [38]. Other studies have also explained the voltage drop of QDSCs due to nonradiative recombination [38–40].

4. Conclusions

We analyzed the DB of the MEGSC with nonradiative recombination. In the ideal MEGSC, the excited electron after AR emits high photon energy under the stringent blackbody radiation condition ($=QY_{max} \cdot E_g$, where QY_{max} is the maximum QY). However, an excited electron in the actual materials loses its kinetic energy through a phonon-assisted cooling process. The NQY from the pump–probe measurements depends on the material status (defects and effective mass), so its related parameters, E_{th} and QY, deviate from IQY.

In the DB of the MEGSC, we introduced the ratio f_{NR} between radiative and nonradiative recombination to see the impact of the ideal reverse saturation current. Typically, $E_{th} = 2E_g$ with $f_{NR} = 10^{-1}$ is the critical point to regard the QD status for the effect of MEG under one-sun illumination. Increasing the light concentration improves MEG. The minimum point for the MEGSC under NQY (in actual material systems) is $f_{NR} = 10^{-4}$ at $E_{th} = 2E_g$, $3E_g$, and $4E_g$. J_0 must be lower than 10^4 times J_0 under full-light concentration to maintain the performance of the MEGSC. We compared the proposed approach with the experimental results to explain the effect of nonradiative recombination on MEGSCs. Minimizing nonradiative recombination can significantly improve V_{OC} by reducing surface defects.

Supplementary Materials: The following are available online at http://www.mdpi.com/2076-3417/10/16/5558/s1, Table S1: The theoretical maximum efficiency with the variation of f_{NR} under one-sun illumination (C = 1), where η is the efficiency. Table S2: The theoretical maximum efficiency for different values of f_{NR} under full-light concentration (C = 46,200), where η is the efficiency. Figure S1: Variations of f_{NR} with theoretical efficiencies of the MEGSC. For this simulation, we use IQY and NQY ($E_{th} = 2 \cdot E_g$, $3 \cdot E_g$, and $4 \cdot E_g$) under one-sun illumination. Figure S2: Variations of f_{NR} with theoretical efficiencies of the MEGSC. For this simulation, we use IQY and NQY ($E_{th} = 2 \cdot E_g$, $3 \cdot E_g$, and $4 \cdot E_g$) under full-light concentration.

Author Contributions: Conceptualization, J.L.; Supervision, C.B.H.; Writing—original draft, J.L.; Writing—review & editing, J.L. All authors have read and agreed to the published version of the manuscript.

Funding: This research paper is based upon work supported in part by the Engineering Research Center Program of the National Science Foundation and the Department of Energy.

Acknowledgments: This research paper is based upon work supported in part by the Engineering Research Center Program of the National Science Foundation and the Office of Energy Efficiency and Renewable Energy of the Department of Energy under NSF Cooperative Agreement No. EEC-1041895. Any opinions, findings, and conclusions or recommendations expressed in this material are those of the authors and do not necessarily reflect those of the National Science Foundation or Department of Energy.

Conflicts of Interest: The authors declare no conflict of interest.

References

1. Shockley, W.; Queisser, H.J. Detailed Balance Limit of Efficiency of p-n Junction Solar Cells. *J. Appl. Phys.* **1961**, *32*, 510. [CrossRef]
2. Green, M.A. Third generation photovoltaics: Solar cells for 2020 and beyond. *Phys. E Low-Dimens. Syst. Nanostruct.* **2002**, *14*, 65–70. [CrossRef]
3. Nozik, A. Quantum dot solar cells. *Phys. E Low-Dimens. Syst. Nanostruct.* **2002**, *14*, 115–120. [CrossRef]
4. Kolodinski, S.; Werner, J.H.; Wittchen, T.; Queisser, H.J. Quantum efficiencies exceeding unity due to impact ionization in silicon solar cells. *Appl. Phys. Lett.* **1993**, *63*, 2405–2407. [CrossRef]
5. Werner, J.H.; Kolodinski, S.; Queisser, H.J. Novel optimization principles and efficiency limits for semiconductor solar cells. *Phys. Rev. Lett.* **1994**, *72*, 3851–3854. [CrossRef]
6. Werner, J.H.; Brendel, R.; Oueisser, H. New Upper Efficiency Limits for Semiconductor Solar Cells. In Proceedings of the 1994 IEEE 1st World Conference on Photovoltaic Energy Conversion—WCPEC (A Joint Conference of PVSC, PVSEC and PSEC), Waikoloa, HI, USA, 5–9 December 1994; pp. 1742–1745.
7. Werner, J.H.; Brendel, R.; Queisser, H.-J. Radiative efficiency limit of terrestrial solar cells with internal carrier multiplication. *Appl. Phys. Lett.* **1995**, *67*, 1028–1030. [CrossRef]
8. Brendel, R.; Werner, J.; Queisser, H. Thermodynamic efficiency limits for semiconductor solar cells with carrier multiplication. *Sol. Energy Mater. Sol. Cells* **1996**, *41*, 419–425. [CrossRef]
9. De Vos, A.; Desoete, B. On the ideal performance of solar cells with larger-than-unity quantum efficiency. *Sol. Energy Mater. Sol. Cells* **1998**, *51*, 413–424. [CrossRef]
10. Franceschetti, A.; An, J.M.; Zunger, A. Impact Ionization Can Explain Carrier Multiplication in PbSe Quantum Dots. *Nano Lett.* **2006**, *6*, 2191–2195. [CrossRef]
11. Zhang, Y.; Wu, G.; Liu, F.; Ding, C.; Zou, Z.; Shen, Q. Photoexcited carrier dynamics in colloidal quantum dot solar cells: Insights into individual quantum dots, quantum dot solid films and devices. *Chem. Soc. Rev.* **2020**, *49*, 49–84. [CrossRef]
12. Beard, M.; Midgett, A.G.; Hanna, M.C.; Luther, J.M.; Hughes, B.K.; Nozik, A.J. Comparing Multiple Exciton Generation in Quantum Dots To Impact Ionization in Bulk Semiconductors: Implications for Enhancement of Solar Energy Conversion. *Nano Lett.* **2010**, *10*, 3019–3027. [CrossRef] [PubMed]
13. Schaller, R.D.; Sykora, M.; Pietryga, J.M.; Klimov, V.I. Seven Excitons at a Cost of One: Redefining the Limits for Conversion Efficiency of Photons into Charge Carriers. *Nano Lett.* **2006**, *6*, 424–429. [CrossRef] [PubMed]
14. Nair, G.; Bawendi, M.G. Carrier multiplication yields of CdSe and CdTe nanocrystals by transient photoluminescence spectroscopy. *Phys. Rev. B* **2007**, *76*, 081304. [CrossRef]
15. Schaller, R.D.; Petruska, M.A.; Klimov, V.I. Effect of electronic structure on carrier multiplication efficiency: Comparative study of PbSe and CdSe nanocrystals. *Appl. Phys. Lett.* **2005**, *87*, 253102. [CrossRef]
16. Pijpers, J.J.H.; Hendry, E.; Milder, M.T.W.; Fanciulli, R.; Savolainen, J.; Herek, J.L.; Vanmaekelbergh, D.; Ruhman, S.; Mocatta, D.; Oron, D.; et al. Carrier Multiplication and Its Reduction by Photodoping in Colloidal InAs Quantum Dots. *J. Phys. Chem. C* **2007**, *111*, 4146–4152. [CrossRef]
17. Schaller, R.D.; Pietryga, J.M.; Klimov, V.I. Carrier Multiplication in InAs Nanocrystal Quantum Dots with an Onset Defined by the Energy Conservation Limit. *Nano Lett.* **2007**, *7*, 3469–3476. [CrossRef]
18. Beard, M.C.; Knutsen, K.P.; Yu, P.; Luther, J.; Song, Q.; Metzger, W.K.; Ellingson, R.J.; Nozik, A.J. Multiple Exciton Generation in Colloidal Silicon Nanocrystals. *Nano Lett.* **2007**, *7*, 2506–2512. [CrossRef]
19. McGuire, J.A.; Joo, J.; Pietryga, J.M.; Schaller, R.D.; Klimov, V.I. New Aspects of Carrier Multiplication in Semiconductor Nanocrystals. *Acc. Chem. Res.* **2008**, *41*, 1810–1819. [CrossRef]
20. Trinh, M.T.; Houtepen, A.J.; Schins, J.M.; Hanrath, T.; Piris, J.; Knulst, W.; Goossens, A.P.L.M.; Siebbeles, L.D.A. In Spite of Recent Doubts Carrier Multiplication Does Occur in PbSe Nanocrystals. *Nano Lett.* **2008**, *8*, 1713–1718. [CrossRef]
21. Beard, M.C.; Midgett, A.G.; Law, M.; Semonin, O.E.; Ellingson, R.J.; Nozik, A.J. Variations in the Quantum Efficiency of Multiple Exciton Generation for a Series of Chemically Treated PbSe Nanocrystal Films. *Nano Lett.* **2009**, *9*, 836–845. [CrossRef]
22. Pijpers, J.J.H.; Ulbricht, R.; Tielrooij, K.-J.; Osherov, A.; Golan, Y.; Delerue, C.; Allan, G.; Bonn, M. Assessment of carrier-multiplication efficiency in bulk PbSe and PbS. *Nat. Phys.* **2009**, *5*, 811–814. [CrossRef]
23. Tyagi, P.; Kambhampati, P. False multiple exciton recombination and multiple exciton generation signals in semiconductor quantum dots arise from surface charge trapping. *J. Chem. Phys.* **2011**, *134*, 94706. [CrossRef]

24. Midgett, A.G.; Hillhouse, H.W.; Hughes, B.K.; Nozik, A.J.; Beard, M. Flowing versus Static Conditions for Measuring Multiple Exciton Generation in PbSe Quantum Dots. *J. Phys. Chem. C* **2010**, *114*, 17486–17500. [CrossRef]
25. Trinh, M.T.; Polak, L.; Schins, J.M.; Houtepen, A.J.; Vaxenburg, R.; Maikov, G.I.; Grinbom, G.; Midgett, A.G.; Luther, J.M.; Beard, M.; et al. Anomalous Independence of Multiple Exciton Generation on Different Group IV−VI Quantum Dot Architectures. *Nano Lett.* **2011**, *11*, 1623–1629. [CrossRef] [PubMed]
26. Beard, M.C.; Johnson, J.C.; Luther, J.; Nozik, A.J. Multiple exciton generation in quantum dots versus singlet fission in molecular chromophores for solar photon conversion. *Philos. Trans. R. Soc. A Math. Phys. Eng. Sci.* **2015**, *373*, 20140412. [CrossRef] [PubMed]
27. Semonin, O.E.; Luther, J.; Choi, S.; Chen, H.-Y.; Gao, J.; Nozik, A.J.; Beard, M.C. Peak External Photocurrent Quantum Efficiency Exceeding 100% via MEG in a Quantum Dot Solar Cell. *Science* **2011**, *334*, 1530–1533. [CrossRef] [PubMed]
28. Davis, N.J.L.K.; Böhm, M.L.; Tabachnyk, M.; Wisnivesky-Rocca-Rivarola, F.; Jellicoe, T.; Ducati, C.; Ehrler, B.; Greenham, N.C. Multiple-exciton generation in lead selenide nanorod solar cells with external quantum efficiencies exceeding 120%. *Nat. Commun.* **2015**, *6*, 8259. [CrossRef]
29. Böhm, M.L.; Jellicoe, T.; Tabachnyk, M.; Davis, N.J.L.K.; Wisnivesky-Rocca-Rivarola, F.; Ducati, C.; Ehrler, B.; Bakulin, A.A.; Greenham, N.C. Lead Telluride Quantum Dot Solar Cells Displaying External Quantum Efficiencies Exceeding 120%. *Nano Lett.* **2015**, *15*, 7987–7993. [CrossRef]
30. Klimov, V.I. Detailed-balance power conversion limits of nanocrystal-quantum-dot solar cells in the presence of carrier multiplication. *Appl. Phys. Lett.* **2006**, *89*, 123118. [CrossRef]
31. Tiedje, T.; Yablonovitch, E.; Cody, G.; Brooks, B. Limiting efficiency of silicon solar cells. *IEEE Trans. Electron Devices* **1984**, *31*, 711–716. [CrossRef]
32. Li, M.; Begum, R.; Fu, J.; Xu, Q.; Koh, T.M.; Veldhuis, S.A.; Grätzel, M.; Mathews, N.; Mhaisalkar, S.; Sum, T.C.; et al. Low threshold and efficient multiple exciton generation in halide perovskite nanocrystals. *Nat. Commun.* **2018**, *9*, 4197. [CrossRef] [PubMed]
33. Karki, K.J.; Ma, F.; Zheng, K.; Žídek, K.; Mousa, A.; Abdellah, M.A.; Messing, M.E.; Wallenberg, L.; Yartsev, A.; Pullerits, T. Multiple exciton generation in nano-crystals revisited: Consistent calculation of the yield based on pump-probe spectroscopy. *Sci. Rep.* **2013**, *3*, 2287. [CrossRef] [PubMed]
34. Beard, M.C.; Ellingson, R. Multiple exciton generation in semiconductor nanocrystals: Toward efficient solar energy conversion. *Laser Photonics Rev.* **2008**, *2*, 377–399. [CrossRef]
35. Hanna, M.C.; Nozik, A.J. Solar conversion efficiency of photovoltaic and photoelectrolysis cells with carrier multiplication absorbers. *J. Appl. Phys.* **2006**, *100*, 074510. [CrossRef]
36. Takeda, Y.; Motohiro, T. Requisites to realize high conversion efficiency of solar cells utilizing carrier multiplication. *Sol. Energy Mater. Sol. Cells* **2010**, *94*, 1399–1405. [CrossRef]
37. Goodwin, H.; Jellicoe, T.; Davis, N.J.L.K.; Böhm, M.L. Multiple exciton generation in quantum dot-based solar cells. *Nanophotonics* **2018**, *7*, 111–126. [CrossRef]
38. Zhu, L.; Lee, K.-H.; Yamaguchi, M.; Akiyama, H.; Kanemitsu, Y.; Araki, K.; Kojima, N. Analysis of nonradiative recombination in quantum dot solar cells and materials. *Prog. Photovolt. Res. Appl.* **2019**, *27*, 971–977. [CrossRef]
39. Wang, Y.; Jia, B.; Wang, J.; Xue, P.; Xiao, Y.; Li, T.; Wang, J.; Lu, H.; Tang, Z.; Lu, X.; et al. High-Efficiency Perovskite Quantum Dot Hybrid Nonfullerene Organic Solar Cells with Near-Zero Driving Force. *Adv. Mater.* **2020**, *32*, 2002066. [CrossRef]
40. Geisz, J.F.; Steiner, M.A.; Garcia, I.; Kurtz, S.R.; Friedman, D.J. Enhanced external radiative efficiency for 20.8% efficient single-junction GaInP solar cells. *Appl. Phys. Lett.* **2013**, *103*, 041118. [CrossRef]
41. Hao, M.; Bai, Y.; Zeiske, S.; Ren, L.; Liu, J.; Yuan, Y.; Zarrabi, N.; Cheng, N.; Ghasemi, M.; Chen, P.; et al. Ligand-assisted cation-exchange engineering for high-efficiency colloidal Cs1−xFAxPbI3 quantum dot solar cells with reduced phase segregation. *Nat. Energy* **2020**, *5*, 79–88. [CrossRef]